

Silicon Photonics at the University of Surrey

G T Reed¹, G Mashanovich¹, F Y Gardes¹, R M Gwilliam¹, N.M.Wright¹, D.J.Thomson¹, B D Timotijevic¹
K.L.Litvinenko¹, W.R.Headley¹, A.J.Smith¹, A P Knights², P E Jessop², N G Tar³, J.H.B.Deane⁴

¹Advanced Technology Institute, University of Surrey,
Guildford, Surrey, GU2 7XH, United Kingdom

²Department of Engineering Physics, McMaster University, 1280 Main Street West,
Hamilton, Ontario, L8S 4L7, Canada.

³Department of Electronics, Carleton University, 1125 Colonel By Drive, Ottawa, Ontario, K1S 5B6, Canada.

⁴Department of Mathematics & Statistics, University of Surrey Guildford, GU2 7XH, UK

ABSTRACT

Silicon Photonics is a field that has seen rapid growth and dramatic changes in the past 5 years. According to the MIT Communications Technology Roadmap [1], which aims to establish a common architecture platform across market sectors with a potential \$20B in annual revenue, silicon photonics is among the top ten emerging technologies. This has in part been a consequence of the recent involvement of large semiconductor companies around the world, particularly in the USA. Significant investment in the technology has also followed in Japan, Korea, and in the European Union. Low cost is a key driver, so it is imperative to pursue technologies that are mass-producible.

Therefore, Silicon Photonics continues to progress at a rapid rate. This paper will describe some of the work of the Silicon Photonics Group at the University of Surrey in the UK. The work is concerned with the sequential development of a series of components for silicon photonic optical circuits, and some of the components are discussed here. In particular the paper will present work on optical waveguides, optical filters, modulators, and lifetime modification of carriers generated by two photon absorption, to improve the performance of Raman amplifiers in silicon.

Keywords: Silicon-On-Insulator (SOI), optical modulators, optical filters, ring resonators, silicon photonics, silicon waveguides

1. INTRODUCTION

Silicon-On-Insulator (SOI) is a practical material for use in fabricating optical devices with a range of applications [e.g. 2-4]. With its large refractive index, stronger optical confinement is possible than in typical oxide-based devices. This confinement allows for relatively small device dimensions so that a higher packing density can be achieved. A further benefit to using this material system comes from the mature field of silicon Ultra Large Scale Integration (ULSI) processing. A combination of the high packing densities with the potential for low-cost fabrication implies that the cost per device can become economically advantageous over some other device technologies.

The field of Silicon photonics has reported some dramatic results over the last several years in terms of lasers [5], high-speed modulators [6, 7], and filtering functions [8], amongst many others. In this paper we discuss some of the work being carried out at the University of Surrey in the UK, and look forward to future work. In particular, in different sections of the paper, work is discussed on novel waveguides and their characteristics, optical filters, optical modulators, and carrier lifetime modification for Raman amplification

2. SILICON WAVEGUIDES

The growing interest in silicon photonic components is motivated in part by the prospect of using well-established and cost effective silicon device processing technology to fabricate components that perform optical. The aim of the current work is the characterization of some novel waveguides. The waveguides are fabricated in silicon-on-insulator (SOI) substrates, using the well-established VLSI technique of the Local Oxidation of Silicon (LOCOS).

2.1 LOCOS Waveguides

Micrometer size waveguide using this process has been demonstrated by Rowe et al [9] reporting low loss (less than 1 dB/cm) as well as the fabrication of an unbalanced Mach-Zehnder device with Y-splitter junctions capable of a 6–10 dB modulation depth in the 1470–1580 nm wavelength range. In this paper, we report submicrometer LOCOS waveguides. We also discuss the fabrication technique and the measurement of optical loss at a wavelength of 1550nm for TE and TM polarizations.

2.1.1 Fabrication:

A p-type SOI wafer, with a 1500 nm silicon overlayer, and a 2.8 micron buried oxide thickness fabricated using the SmartCut[®] technique, was used as the starting material. The wafer was thinned using thermal oxidation and subsequent etching in buffered HF acid to obtain an overlayer thickness of around 650 nm +/- 20nm. Following the growth of a 40 nm SiO₂ pad oxide, a Si₃N₄ masking layer of 80 nm was deposited by Low Pressure Chemical Vapor Deposition (LPCVD). Trenches in the Si₃N₄ layer were then defined by photolithography and plasma etch (Figure 1a). Following removal of the photoresist, the structure was wet-oxidized to produce a 410 nm thick SiO₂ layer in the unmasked trench areas (Figure 1b). Finally the Si₃N₄ layer was removed revealing an optical waveguide between the oxidized trenches (Figure 1c). The fabrication process is illustrated in Figure 1, whilst Figure 2 shows an SEM cross section of one of the fabricated waveguides. Of some importance, the sidewalls of the waveguide have an angle of 22° in relation to the substrate, however we note that this angle could be increased significantly by the use of modified LOCOS processes such as SWAMI [10].

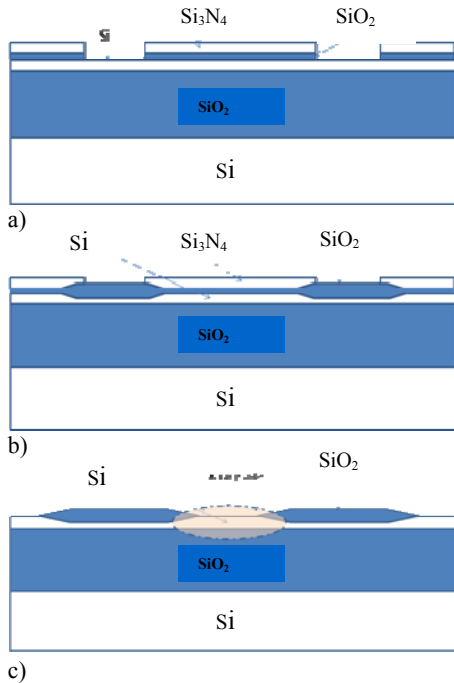


Figure 1 LOCOS waveguides process (a,b,c)

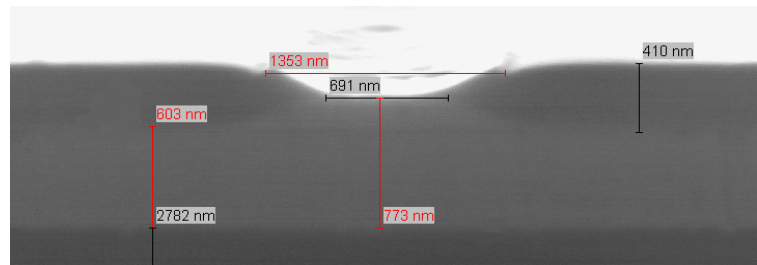


Figure 2 SEM of the measured waveguides

2.1.2 Experimental measurements

The waveguides were measured using the well known Fabry–Perot technique [11]. On the test chip, the facets were not anti reflection coated, therefore the light propagates along the waveguide and is reflected at both facets by an amount determined by the refractive index of the waveguide material (silicon) and the external material (air). The waveguide structure is then regarded as a resonant or Fabry-Perot cavity [11]. By using the light intensity transmitted through such a cavity it has been possible to calculate the loss coefficient. The optical loss has been measured for TE and TM polarisation input state and for each input polarisation, the output power was filtered into both states. The loss measured for TE-TE polarisation, for a length of 9.5 mm was 0.32 dB/cm, 0.21 dB/cm, 0.26 dB/cm respectively for waveguide widths of 1.1, 1.5, 1.7 μm at a wavelength of 1550nm. The losses of the pure polarisation transmissions and their conversions are shown on figure 3. It is clear that pure TE transmission is almost unaffected by the variation of the width

of the waveguide where the loss is contained in a range going from 0.2 to 2 dB/cm. Pure TM transmission, however, is affected and varies from 3dB/cm to more than 15 dB/cm for the lowest waveguide width measured.

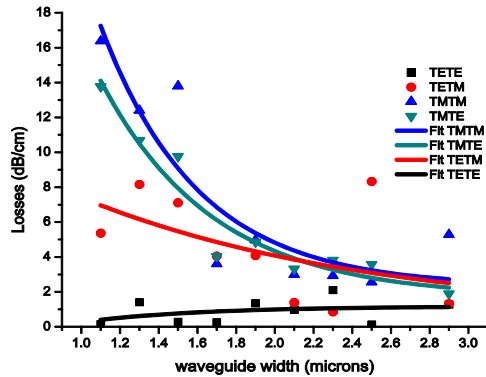


Figure 3 Polarisation losses against waveguide width.

3. FILTERS

We have previously produced polarisation independent devices based upon rib waveguides, which result in ring resonators with large dimensions [8]. This in turn results in a small free spectral range (FSR), which is acceptable for some modulator applications, but is not useful for filtering functions. Therefore we have carried out work on optical filters based upon strip waveguide based ring resonators, attempting to produce both a large FSR device, and also to control the polarisation performance.

The simplest ring resonator based filter is a single resonator. It consists of a resonator and a straight waveguide acting as an input/output (through) port. A second straight waveguide can be added to observe the spectrum at a second output also known as the drop port. Whilst single rib waveguide based resonators cannot give very large FSRs, typically up to a few nanometres, the devices based upon strip waveguides are capable of producing relatively large FSRs, over 10s of nm. Therefore, it is worth considering a single resonator structure. We have previously reported small optical filters with an FSR as large as 43 nm (figure 4) [13] and subsequently 62 nm [14]. In this work, other important parameters are extinction ratio (12.6), and FWHM, estimated to be ~ 3.1 nm at 1540 nm and ~ 5.5 nm at 1586 nm.

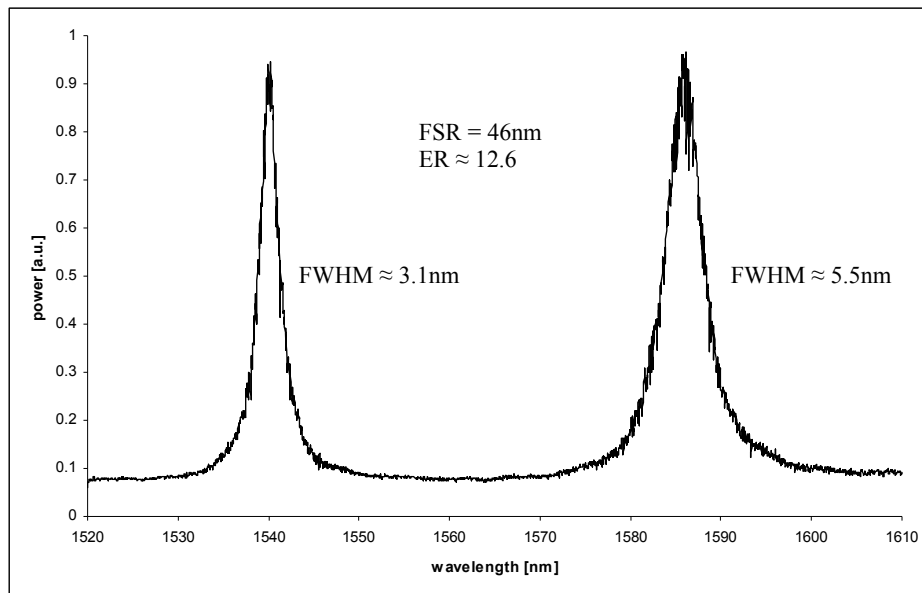


Figure 4 TE response of a 2µm ring at the drop port. The FSR is ~ 46 nm

The large FSR of 62 nm has been obtained by using 1.5 μm radius rings, the resultant response being shown in figure 5. The same figure shows that stability of the response might be an issue. The second graph in Figure 5 shows the response of a similar device, where the same geometric parameters have been used, but the device is from a different test chip for which slightly different exposure recipes were utilised during the lithography process in order to fabricate target devices. It can be seen that the FSR is not affected, but a shift of ~ 9 nm has been introduced. Considering that the modes are very likely to react differently to the change, polarisation insensitivity can be significantly altered. Thus, very accurate waveguide and device layouts are prerequisites for stable responses and good control over the polarisation performance.

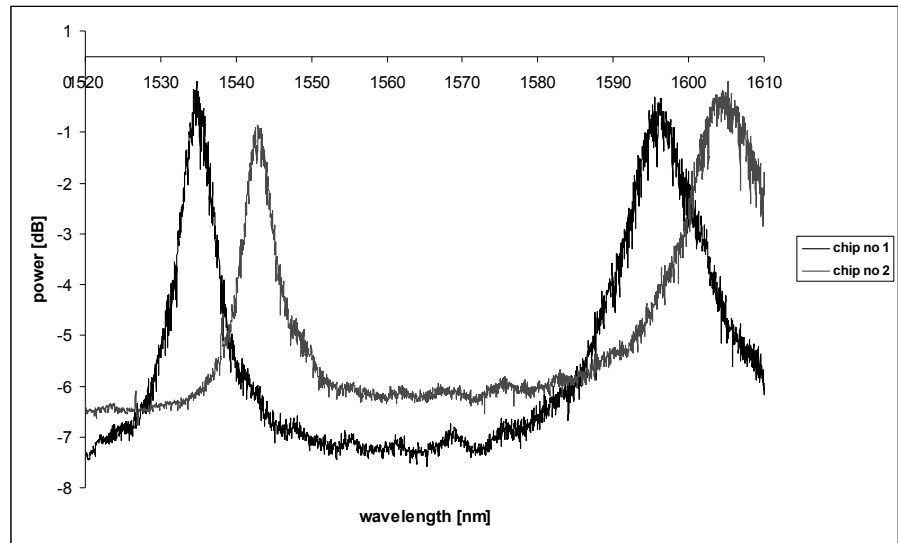


Figure 5 The responses of 1.5 μm rings with identical parameters but slightly different lithography exposures. The resonators are made of waveguides which width is 380nm and height 290nm. The obtained FSR is ~ 62 nm

By utilising ring resonator waveguides with the following parameters, height = 290 nm, width = 380 nm, coupler separation = 100 nm, ring radius = 3 μm , we have also attempted to produce polarisation independent devices. Whilst such devices are sensitive to processing inaccuracies, and thermal fluctuations, figure 6 shows that reasonable results can be produced.

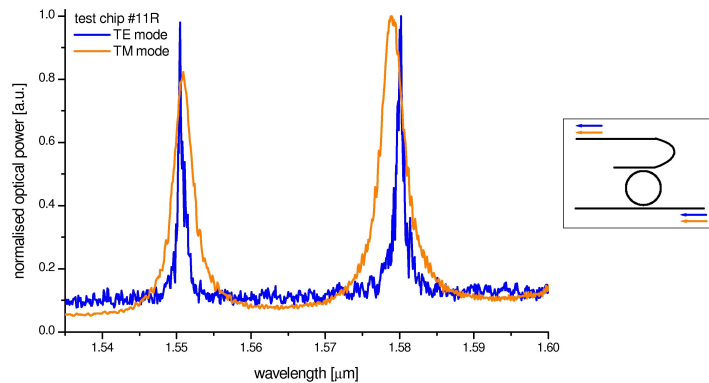


Figure 6 Close to polarization independent ring resonator performance based upon 3 μm radius.

4. MODULATORS

Whilst we have worked on a range of optical modulators in silicon, in recent years we have concentrated on depletion devices [e.g.15, 16]. One of our approaches was to provide a design to obtain high modulation speed and polarisation independence in a single mode waveguide, as demonstrated in [8] and improve the efficiency of optical modulators using a V-shaped pn junction based on the natural etch angle of silicon, 54.7 degrees [16].

The V-shaped pn junction was compared to a flat horizontal junction situated in the centre of the waveguide, hence enabling the possibility to measure the evolution of the TE and TM polarisation during modulation in both cases. The dimensions of both modulators are as follows: height, $H=1.35 \mu\text{m}$, width, $W=1 \mu\text{m}$ and etch depth, $E=0.83 \mu\text{m}$. This design was chosen to provide birefringence free operation for TE and TM polarisations and was reported in [15]. The modulator active structures are based on a horizontal pn junction. A wing design top contact made of polysilicon was proposed by Liao et al for the MOS capacitor modulator [6], and was added on top of the rib to form the P type resistive contact. The N type resistive contact is situated in the slab. The modulation of the pn junction is achieved by applying a reverse bias varying from 0 to 5 volts. The overlap between the optical mode and the change in carrier concentration in the waveguide will create a change in the effective index of the mode propagating in the waveguide. The issue is that the change in the carrier concentration inside the waveguide is not uniform, hence affecting the two polarisations in different ways. The goal in this specific case was to find a junction architecture that would improve the efficiency and allow polarisation independence during modulation.

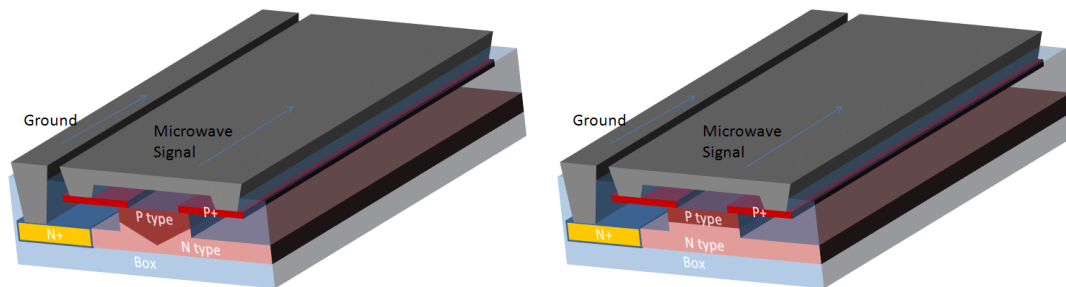


Figure 7 Micrometer size modulators with V-shaped pn junction and flat pn junction.

Figure 7 shows the profile of the proposed modulators. In order to study the birefringence and compare them to one another, in both modulators the height of the junction was varied and the change in phase shift for a length of 5 millimeters was calculated for voltages varying between 0 and 5 volts in reverse bias. The results are shown in figure 8.

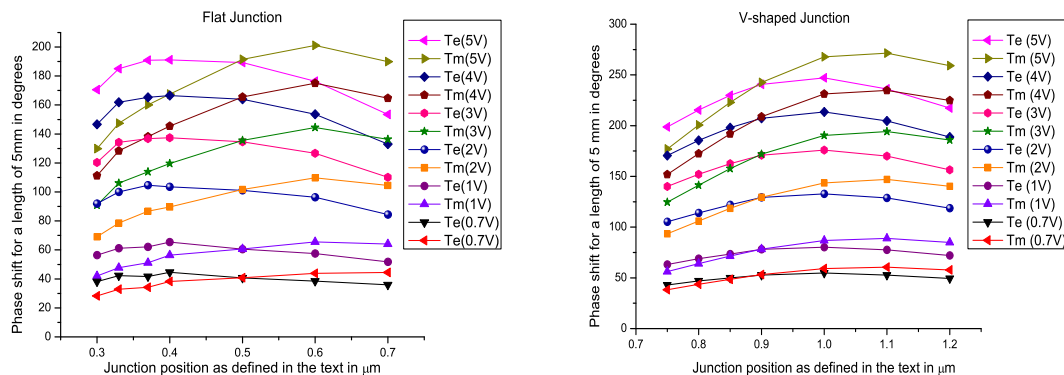


Figure 8 Study of the birefringence during modulation for the flat and v-shaped junction when the height of the pn junction is varied.

Birefringence free modulation is achievable for both modulators. In the case of the flat junction it is achieved for a junction height of 0.5 microns which correspond roughly to the interface between the rib and the slab, and for the V shaped junction, the birefringence free condition is achieved at a height of 0.87 microns. Although birefringence free performance is achievable in the case of the flat junction the fabrication tolerance is tight and the difference between TE and TM modulation increase rapidly if the junction depth is not accurately fabricated. On the other hand, the V-shaped junction will have a better resilience to fabrication tolerances. Furthermore the V-shaped junction has a better efficiency $L_{\pi} \cdot V_{\pi} = 2.5 \text{ V.cm}$ compared to $L_{\pi} \cdot V_{\pi} = 3.1 \text{ V.cm}$ for the flat junction. The efficiency of a modulator comes from the overlap of the mode profile and the refractive index variation due to the carrier distribution change. Hence the more carriers that are removed from the overlap region for a specific reverse bias, then the better the efficiency will be. The p-type region, also play an important role in the efficiency as the concentration holes plays a more dominant role than the concentration of electrons in the refractive index change. Intuitively one would expect TE and TM modes to be affected equally if a junction could be fabricated at 45 degrees to the major TE and TM axes if the TE and TM axes were identical, but simply rotated by 90 degrees with respect to one another. However, because the mode shapes are different, some other angle is likely to be optimal. However, the flat junction will definitely not be optimal and will probably show the most extreme polarisation dependence. That can be mitigated to some extent, by translation of the junction vertically. Thus it is not surprising that the flat junction shows more polarisation dependence than the V-shaped junction, which in turn, must be nearer to the optimal angle than the flat junction. The V-shaped junction will also be more phase efficient than the flat junction, simply because the V-shape results in a greater net length of the junction and hence in more net depletion.

The intrinsic bandwidth for both modulators was determined with the junctions positioned in order to achieve birefringence free during modulation. The voltage sweep applied was 10 volts with a voltage rise time of 1 picosecond. The birefringence free condition is also conserved during modulation as is shown by figure 9. The V-shape junction has a rise time of 13 ps and a fall time of 23 ps for both TE and TM. For the flat junction the rise time is 12 ps and the fall time is 21 ps for both TE and TM. In both cases, this corresponds to an intrinsic bandwidth in excess of 15 GHz.

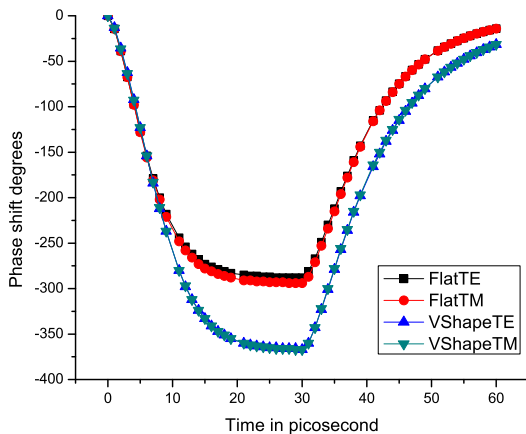


Figure 9 Phase shift against transient time for TE and TM for the flat junction and the V-shaped junction.

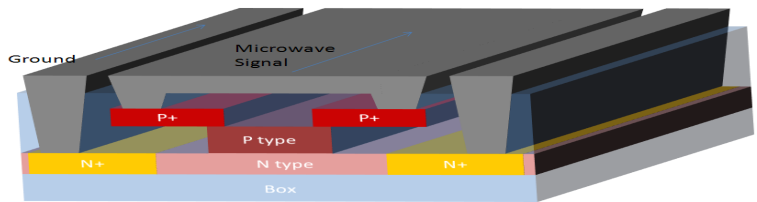


Figure 10 Schematic cross-section of SOI sub micrometer rib waveguide with an integrated three terminal p-n diode for plasma dispersion modulation [15].

The prospect of a micrometer size silicon on insulator modulator, able to achieve an intrinsic bandwidth in excess of 15 GHz while maintaining birefringence free during modulation with an efficiency $L_{\pi} \cdot V_{\pi} = 2.5 \text{ V.cm}$ is very promising, but still some aspects have scope for improvement. For instance, the loss due to the doped area (1×10^{18} for p and n regions) is above 10 dB/cm and the size of the device (5 mm) too long for highly integrated devices, furthermore the power requirements during high speed modulation can be in the order of a few watts. In order to increase efficiency, modulation speed, the intrinsic loss figure, and a higher integration prospect a decrease in the size of the device is necessary.

In order to maximise the overlap of the mode profile and the depletion area of the pn junction, a sub micrometer size rib waveguide was proposed in 2005 by Gardes et al in [15] (Figure 10). The device has an asymmetrical p-n structure where two slab regions are joined as a common cathode and two poly-silicon regions are joined as a common anode. It is referred to as a p+pnn+ device for obvious reasons. Both n+ and p+ regions were modelled as highly doped regions with peak doping concentrations of 1×10^{19} ions/cm³ in order to insure a resistive contact. The structure is based on a silicon overlayer thickness of 0.515 microns, 0.45 microns etched rib waveguides, 0.415 microns wide with a slab thickness of 0.10 microns. The silicon slab and the bottom part of the rib have an n-type background doping concentration of 4×10^{17} ions/cm³ and the top part of the rib has a p-type background doping concentration of 2×10^{17} ions/cm³. The oxide thickness was chosen to be 1 mm which ensures sufficiently good optical confinement and a top silicon oxide cladding layer covers the whole structure. The n⁺ doped regions are situated on both sides of the waveguiding region, in the slab, 1.5 microns away from the centre of the waveguide. Furthermore the poly-silicon p+ doped regions are situated on both sides of the top of the rib in order to reduce the loss resulting from the poly-silicon and aluminium contacts. This specific waveguide configuration enables us to approach birefringence free performance for TE and TM polarisations and a higher confinement of the mode in the waveguide. Hence the simulation results in terms of efficiency are greatly improved with a $L_{\pi} \cdot V_{\pi} = 2.5$ V.cm, whilst a low doping concentration around 4 and 2×10^{17} ions/cm³ was used for electrons and holes compared to 1×10^{18} ions/cm³ in the case of a micrometer waveguide. This greatly improves the loss figure of the modulator varying from 2dB for 2.5 mm active length to 1dB for 2.5 mm active length for a reverse voltage of 0 and 10 volts respectively. Furthermore the switching time has been greatly improved and the rise and fall times calculated are in the order of 7 ps for a switch bias of only 5 volts (in a push pull configuration).

This has shown the possibility of improving the characteristics of depletion modulators in terms of efficiency/ loss factor as well as a major increase in bandwidth enabling modulation above 50 GHz. A similar modulator structure operating on this principle has now been demonstrated by Liu et al [17], with 30 GHz bandwidth and a 4 V.cm efficiency.

However, several issues still remain. For instance the power requirements for the sub micrometer device are measured in watts at full speed; this means that more than 1 Amp of peak current has to be delivered to the device. Furthermore the fabrication of a sharp horizontal pn junction is difficult to achieve by using ion implantation and requires the use of doped silicon epitaxial overgrowth process as suggested in [17]. This is obviously a long, complicated, development intensive and expensive process which requires many fabrication steps. In order to resolve the fabrication issues due to the need of applying a top contact to a rib waveguide, a structure containing a lateral pn junction can be realised. This enables the simplification of the process by forming the junction using ion implantation. Also the multiple steps required by the formation of a top contact are not necessary, and a simple rib etch is necessary to form the waveguide. Furthermore the mode mismatch between the interface of the active area of the modulator and the waveguide will be negligible as the structure is intrinsically the same if one neglects the implanted ions. This should also reduce the insertion loss of the modulator.

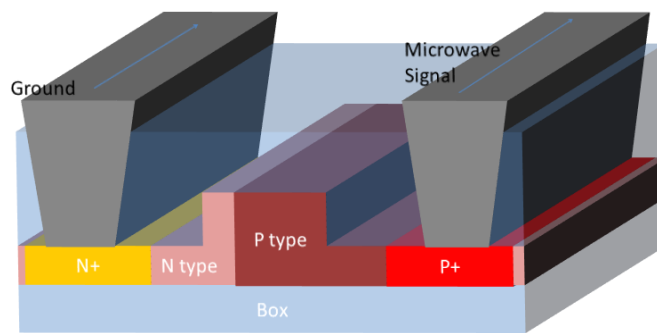


Figure 11 Schematic cross-section of SOI sub micrometer rib waveguide with an integrated two terminal lateral p-n diode for plasma dispersion modulation.

Figure 11, schematically shows such a modulator and is being developed in a project collaboration regrouping European universities and companies via a European network, ePIXnet [18]. The device is based on a 300 nm wide, 150nm etch depth and 200 nm high rib waveguide. The Resistive contacts are placed 1 micron away from the junction in order to

minimise interaction with the optical mode and hence minimise the losses. The pn junction is asymmetrical in size and in doping concentration in order to maximize overlap area of the optical modes and holes. The N type region is 75 nm wide and the P type 225 nm wide, the net doping of the junction is approximately $1 \times 10^{18}/\text{cm}^3$ and $4 \times 10^{17}/\text{cm}^3$, for N and P type respectively. The highly doped regions are doped to $1 \times 10^{20}/\text{cm}^3$ in order to form a good resistive contact. The main fabrication concern for this device is the formation of the pn junction. As the waveguide width is 300 nm, two problems arise. The first one is to align the implantation mask of the N type doping and waveguide etch such that the junction is formed inside the waveguide with sufficient width in order to enable an efficient depletion process. The second issue is the diffusion of carriers due to activation annealing. In this regard the Boron was chosen for the background P type doping, BF₂ for the shallow resistive contact and Antimony for the N type doping. Antimony was chosen for its low diffusion characteristics and is implanted in a P type boron $4 \times 10^{17}/\text{cm}^3$ background, hence forming the sharp vertical pn junction required for this particular device.

The calculated characteristics of this specific device were simulated using Athena for the process development and ion implantation steps, and Atlas for DC and transient analysis, both part of the semiconductor CAD software Silvaco. Optical characteristics for the loss, efficiency and transient analysis were calculated using an in house mode solver and results were reported in [16, 19].

Figure 12 represents the variation of the effective index for a different reverse voltage; the loss of the active area is also displayed, and varies from 13 dB/cm when no bias is applied, to about 7 dB/cm with a reverse bias of 10 volts. The efficiency of this specific modulator is $L_{\pi} \cdot V_{\pi} = 2.23 \text{ V} \cdot \text{cm}$ and is similar to the efficiency of the horizontal version of the modulator. Also a length of 2.23 mm is necessary to obtain a π phase shift with a 10 volt reverse bias. In these conditions the losses due to the doping in the active area of the modulator vary between 1.5 dB and 2.8 dB again very similar to what was calculated for the horizontal junction device.

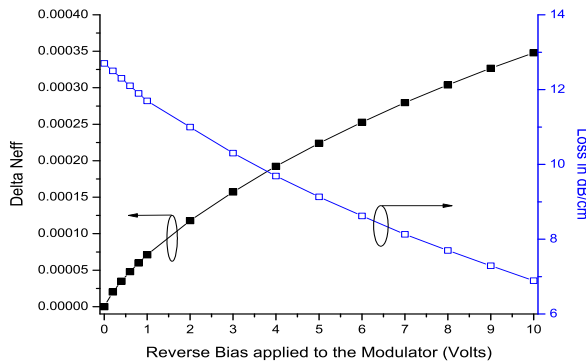


Figure 12 Change in the effective index and losses with reverse bias

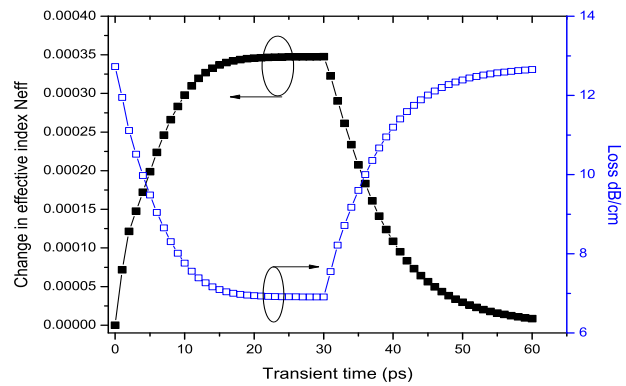


Figure 13 Evolution of the effective index and loss when a reverse bias of 10 volts is applied.

The transient characteristics of the device are displayed in figure 13 and with a switching time of around 25 ps the bandwidth is in excess of 25 GHz. The proposed lateral junction is a much simplified device in order to achieve high speed modulation. The characteristics are similar to previous devices, which makes it a very interesting candidate to achieve high speed modulation in SOI. Furthermore this configuration offers a very simple way to mount the junction in a push pull configuration hence reducing the length of the active area to about 1.1 mm.

5. MODIFICATION OF CARRIER LIFETIME

The Raman effect has been used successfully to produce a silicon laser [20], however very high intensity pump lasers are required to generate amplification due to a non-linear effect known as two-photon-absorption (TPA) [21] which causes free-carrier absorption (FCA) loss that can exceed Raman gain as well as depleting pump photons. P-i-N structures have been used as one way to remove these carriers, and hence reduce the effective carrier lifetime. Scaling the waveguide to sub-micrometer sized dimensions can also reduce the effective lifetime due to enhanced surface recombination [22, 23], although this increases the difficulty of coupling both pump and signal beam to the waveguide. It has already been

shown that implanting helium into rib waveguides [24] can reduce the carrier lifetime without a drastic increase in the propagation loss. A net gain of 0.065dB was measured without the need for a reverse bias to remove the photo-generated free carriers. In this paper we discuss the use of ion induced defects to trap the carriers generated from the TPA process, and the effect of the implanted defects on propagation inside the waveguide

5.2 Experimental results

The silicon rib waveguides were fabricated on (100) SOI wafer. The rib target dimensions were rib width (w) 1µm and height (h) 1.35µm. The waveguides had a length of 8 mm. Ion implantation modeling was carried out in ATHENA [25] to find the damage range in relation to the rib waveguide. The depth of the implanted damage will have an effect on both the free carrier lifetime and the optical loss inside the waveguide. Ion implantation energies were chosen that gave a range of damage depths into the rib waveguide. These ranged from surface implants to fully implanted waveguides. Ion dose (hence defect concentration) was also investigated. The experimental investigation consisted of measurement of excess optical loss introduced by the implanted silicon ions and the measurement of any reduction in free carrier lifetime caused by the implanted ions. Using a broadband source with wavelength range of 1530 nm to 1610 nm, optical absorption measurements were performed. Each waveguide on a specific test chip had a predefined implanted length which varied from fully implanted (8000 microns) to un-implanted. Output power was compared against implanted length to calculate the excess loss introduced for the chosen energy and dose implant. Table 1 summarizes the energy and dose implants used in our experiments, the associated excess propagation loss in dB/cm is also shown. The data was measured a total of 12 times, with the mean value used in the table and the standard error used for error bars.

Table 1. Propagation loss in dB/cm for associated energy and dose implants

Energy keV	Dose cm ⁻²				
	1x10 ¹⁰ cm ⁻²	1x10 ¹¹ cm ⁻²	5x10 ¹¹ cm ⁻²	1x10 ¹² cm ⁻²	1x10 ¹³ cm ⁻²
400	n/a	0.19±0.02	0.25±0.03	0.54±0.07	n/a
750	0.24±0.02	1.38±0.06	6.56±0.17	11.56±0.2	78.02±0.99
1150	0.55±0.09	4.11±0.05	22.38±0.14	35.59±0.19	167.39±1.5
1575	1.91±0.04	4.62±0.05	27.50±0.36	53.18±0.47	n/a
2000	1.61±0.17	4.99±0.04	25.14±0.25	38.94±0.47	171.94±1.1

Two separate implant experiments were performed to collect data for table 1. The first set of experimental results can be seen in bold. Due to the excessive losses seen with the 1x10¹³cm⁻² dose, it was not repeated for the second set of data to be collected. The second set of data to be collected aimed to fill in some of the gaps in the original energy and dose matrix. This allowed for a more comprehensive data set. Figure 14 compares excess loss introduced by ion implantation against dose on a log scale, for different energies.

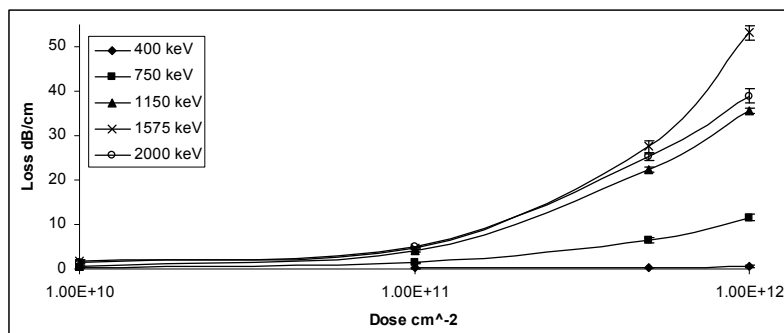


Figure 14 Experimental data comparing excess loss and dose for different energy silicon implant energies

From figure 14 it should be clear that as dose increases, so does the excess loss introduced to the waveguide. Loss also increases for an increased energy, until the defect peak passes through the device into the buried oxide below (2000 keV). Using the same broadband source as before, carrier lifetime measurements were performed for each chip. The experimental setup for lifetime measurements was essentially the same as for the optical loss measurements, but with the addition of a femto-second pulsed laser directed onto the top of the waveguide through a periscope. Figure 15 shows a

diagram of the experimental technique used. Directing the pump beam from above, onto the waveguide being measured, allowed both implanted and un-implanted regions to be measured independently, giving an accurate indication of the lifetime change, since this method allowed near simultaneous investigation of implanted and un-implanted regions, and hence near identical experimental conditions.

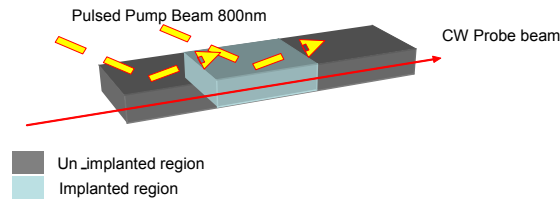


Figure 15. Simplified free carrier lifetime measurement technique. The femto laser is fired onto the waveguide. This excites carriers which attenuate the broadband beam. During the off cycle of the pump, the carriers recombine.

The generation and exponential recovery of carriers was then displayed on a digital oscilloscope via a 12 GHz fibre coupled detector. Origin [26] was used to calculate the free carrier lifetime from the exponential decay of the waveform, using an exponential fitting tool. Table 2 summarizes the percentage reduction in free carrier lifetime caused by the different energy and dose implants. The average un-implanted free carrier lifetime was ~4ns. The gaps in the table were due to excess loss preventing the detector from detecting a signal.

Table 2. Percentage reduction in free carrier lifetime for labeled dose and energy

Energy keV	Dose cm ⁻²			
	1x10 ¹⁰ cm ⁻²	1x10 ¹¹ cm ⁻²	5x10 ¹¹ cm ⁻²	1x10 ¹² cm ⁻²
400	n/a	72.5	79.5	85.4
750	71.27	86.15	93.74	94.021
1150	56.22	86.55	94.47	
1575	55.011	88.15		
2000	52.171	88.46		

The largest percentage reduction in lifetime was 94.47%; this gave a lifetime of 0.23 ns. However the excess loss introduced to the waveguide was ~22.38 dB/cm. Utilizing the lowest energy yields an 85.4% reduction in lifetime (0.56 ns) for only ~0.54 dB/cm excess loss. Figure 16 displays excess loss data for 400 keV implant energy compared with the percentage reduction in free carrier lifetime. The carrier lifetime for each corresponding dose is also shown.

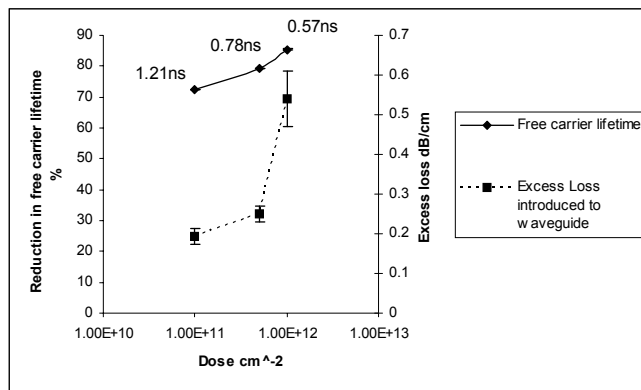


Figure 16 Plot comparing excess loss and reduction in free carrier lifetime for 400keV energy with 10¹¹, 5x10¹¹ and 10¹²cm⁻² doses. As the concentration of defects increases so does the excess loss and reduction in free carrier lifetime.

6. CONCLUSIONS

A series of devices have been presented that have recently been studied at the University of Surrey. These components may offer contributory solutions to low cost optical circuits in silicon photonics, for a range of applications. Promising devices will be taken forward for potential integration both with other optical devices, and in the longer term with drive, electronics, for a range of potential applications. The devices offer the potential of good to moderate performance at low cost, particularly for some devices in which mass production techniques can further reduce cost.

7. ACKNOWLEDGEMENTS

We are grateful to EPSRC and the Intel Corporation for funding. This work was partially funded under the EPSRC programme "UK Silicon Photonics".

REFERENCES

1. <http://mph-roadmap.mit.edu/index.php>
2. Q Xu, B Schmidt, S Pradhan, M Lipson, *Micrometre-scale silicon electro-optic modulator*, Nature, **435**, 325-327, 2005.
3. G. T. Reed, *Silicon optical modulators*, Materials Today, **8**, 40 – 50, 2005.
4. G. Z. Masanovic, G. T. Reed, W. Headley, B. Timotijevic, V. M. N. Passaro, R. Atta, G. Ensell, and A. G. R. Evans, *A high efficiency input/output coupler for small silicon photonic devices*, Opt. Express, **13**, 7374-7379, 2005.
5. H. Rong, A. Liu, R. Nicolaescu, R. Jones, M. Paniccia O. Cohen, D. Hak, *An all-silicon Raman laser*. Nature, **433**,292-294, 2005.
6. A. Liu, R. Jones, L. Liao, D. Samara-Rubio, D. Rubin, O. Cohen, R. Nicolaescu, and M. Paniccia, *A high-speed silicon optical modulator based on a metal-oxide-semiconductor capacitor*, Nature, **427**, 615-618. 2004.
7. F. Y. Gardes, G. T. Reed, N. G. Emerson, and C. E. Png, *A sub-micron depletion-type photonic modulator in Silicon On Insulator*, Opt. Express **13**, 8845-8854, 2005.
8. W. R. Headley, G. T. Reed, S. Howe, A. Liu, and M. Paniccia, *Polarization-independent optical racetrack resonators using rib waveguides on silicon-on-insulator*. Appl. Phys. Lett., **85**, 5523-5, 2004.
9. L. K. Rowe, M. Elsey, N. G. Tarr, A. P. Knights, and E. Post, *"CMOS-compatible optical rib waveguides defined by local oxidation of silicon,"* Electronics Letters, vol. 43, pp. 392-393, 2007.
10. C. Kuang Yi, J. L. Moll, and J. Manoliu, *"A bird's beak free local oxidation technology feasible for VLSI circuits fabrication,"*IEEE Transactions on Electron Devices, vol. 29, pp. 536-540, 1982.
11. G. T. Reed and A. P. Knights, *Silicon Photonics: An Introduction*: John Wiley & Sons, Inc., 2004.
12. W. R. Headley, G. T. Reed, S. Howe, A. Liu, and M. Paniccia, *Polarisation-independent optical racetrack resonators using rib waveguides on silicon-on-insulator*, Appl. Phys. Lett, vol. 85, pp. 5523-5, 2004.
13. B. D. Timotijevic, G. T. Reed, R. Jones, A. Michaeli, A. Liu, and G. Z. Mashanovich, *Small optical filters in silicon-on-insulator*, 3rd Int. Conf. Group IV Photonics, , pp. 25-27, Ottawa, Canada, 2006.
14. B. D. Timotijevic, D. Thomson, F. Y. Gardes, S. Howe, A. Michaeli, J. V. Crnjanski, V. M. N. Passaro, G. Z. Mashanovich, and G. T. Reed, *"Tailoring the response and temperature characteristics of multiple serial-coupled resonators in Silicon on Insulator"*, Silicon Photonics Symposium, SPIE Photonics West, San Jose, California, January 2007.
15. F. Y. Gardes, G. T. Reed, N. G. Emerson, and C. E. Png, *"A sub-micron depletion-type photonic modulator in silicon on insulator,"* Optics Express, vol. 13, 2005.
16. F. Y. Gardes, K. L. Tsakmakidis, D. Thomson, G. T. Reed, G. Z. Mashanovich, O. Hess, and D. Avitabile, *"Micrometer size polarisation independent depletion-type photonic modulator in silicon on insulator,"* Optics Express, vol. 15, pp. 5879-5884, 2007.
17. L. Liao, L. Liao, A. Liu, D. Rubin, J. A. B. J. Basak, Y. A. C. Y. Chetrit, H. A. N. H. Nguyen, R. A. C. R. Cohen, N. A. I. N. Izhaky, and M. A. P. M. Paniccia, *"40 Gbit/s silicon optical modulator for highspeed applications,"* Electronics Letters, vol. 43, 2007.
18. ePIXnet, "European FP6 network of excellence," 2008.
19. K. L. Tsakmakidis, C. Hermann, A. Klaedtke, C. A. J. C. Jamois, and O. Hess, *"Systematic modal analysis of 3-D dielectric waveguides using conventional and high accuracy nonstandard FDTD algorithms,"* IEEE Photonics Technology Letters, vol. 17, pp. 2598-2600, 2005

20. H. Rong, R. Jones, A. Liu, O. Cohen, D. Hak, A. Fang, M. Paniccia, "A continuous-wave Raman silicon laser," *Nature*. **433** 725-728 (2005).
21. R. Claps, V. Raghunathan, D. Dimitropoulos, B. Jalali, "Influence of nonlinear absorption on Raman amplification in Silicon waveguides," *Opt. Express* **12**(12) 2774-2780 (2004).
22. R. L. Espinola, J. I. Dadap, R. M. Osgood, Jr., S. J. McNab, Y. A. Vlasov, "Raman amplification in ultrasmall silicon-on-insulator wire waveguides," *Opt. Express* **12** 3713 (2004).
23. D. Dimitropoulos, R. Jhaveri, R. Claps, J. C. S. Woo, B. Jalali, "Lifetime of photogenerated carriers in silicon-on-insulator rib waveguides," *Appl. Phys. Lett.* **86** 071115 (2005).
24. Y. Liu, H. K. Tsang, "Nonlinear absorption and Raman gain in helium-ion-implanted silicon waveguides," *Opt. Lett.* **31**(11) 1714-16 (2006).
25. Silvaco International, 4701 Patrick Henry Drive, Bldg 1, Santa Clara, CA 94054, www.silvaco.com
26. B. Jalali, V. Raghunathan, D. Dimitropoulos, O. Boyraz, "Raman-based silicon photonics," *IEEE J. Sel. Top. Quantum Electron.* **12**, 412-421 (2006).